Adamantylidene Addition to $M_3N@I_h$-C_{80} (M = Sc, Lu) and $Sc_3N@D_{5h}$-C_{80}: Synthesis and Crystallographic Characterization of the [5,6]-Open and [6,6]-Open Adducts

Michio Yamada,[a] Tsuneyuki Abe,[b] Chiharu Saito,[b] Toshiki Yamazaki,[b] Satoru Sato,[b] Naomi Mizorogi,[b] Zdenek Slanina,[b,c] Filip Uhlík,[d] Mitsuaki Suzuki,[a,e] Yutaka Maeda,[a] Yongfu Lian,[f] Xing Lu,[g] Marilyn M. Olmstead,*[h] Alan L. Balch,*[h] Shigeru Nagase,*[i] and Takeshi Akasaka*[a,b,f,j]

[a] Prof. Dr. M. Yamada, Dr. M. Suzuki, Prof. Dr. Y. Maeda
Department of Chemistry, Tokyo Gakugei University, Tokyo 184-8501 (Japan)
[b] T. Abe, C. Saito, T. Yamazaki, Dr. S. Sato, Dr. N. Mizorogi, Prof. Dr. Z. Slanina
Life Science Center of Tsukuba Advanced Research Alliance, University of Tsukuba, Ibaraki 305-8577 (Japan)
E-mail: akasaka@tara.tsukuba.ac.jp
[c] Prof. Dr. Z. Slanina
Department of Chemistry and Biochemistry National Chung-Cheng University, Chia-Yi 62117 (Taiwan R.O.C.)
[d] Prof. Dr. F. Uhlík
Department of Physical and Macromolecular Chemistry, Charles University in Prague, 128 43 Prague 2, Czech Republic
[e] Prof. Dr. M. Suzuki
Department of Chemistry, Faculty of Science, Josai University, Saitama 350-0295, Japan
[f] Prof. Dr. Y. Lian
Key Laboratory of Functional Inorganic Material Chemistry, Ministry of Education, School of Chemistry and Materials Science, Heilongjiang University, Harbin 150080 (P.R.China)
[g] Prof. Dr. X. Lu
State Key Laboratory of Materials Processing and Die & Mold Technology, School of Materials Science and Engineering, Huazhong University of Science and Technology, Wuhan 430074 (P.R.China)
[h] Prof. Dr. M. M. Olmstead, Prof. Dr. A. L. Balch
Department of Chemistry, University of California, Davis, California 95616 (USA)
E-mail: mmolmstead@ucdavis.edu
albalch@ucdavis.edu
[i] Prof. Dr. S. Nagase
Fukui Institute for Fundamental Chemistry, Kyoto University, Kyoto 606-8103 (Japan)
E-mail: nagase@ims.ac.jp
[j] Prof. Dr. T. Akasaka
Foundation for Advancement of International Science, Ibaraki 305-0821 (Japan)

Supporting information for this article is given via a link at the end of the document.

Abstract: Adamantylidene (Ad) additions to $M_3N@I_h$-C_{80} (M = Sc, Lu) and $Sc_3N@D_{5h}$-C_{80} were conducted comprehensively by photochemical reactions with 2-adamantane-2,3'-[3*H*]-diazirine (**1**). In $M_3N@I_h$-C_{80}, the addition caused the rupture of the [6,6]- or [5,6]-bonds of the I_h-C_{80} cage, forming [6,6]-open fulleroids as a major isomer and [5,6]-open fulleroids as a minor isomer. In $Sc_3N@D_{5h}$-C_{80}, the addition also proceeded regioselectively to yield three major isomers of Ad mono-adducts, despite the fact that nine types of C–C bonds exist in the D_{5h}-C_{80} cage. The molecular structures of the seven Ad mono-adducts, including the positions of encaged trimetallic nitride clusters,

were determined unambiguously using single-crystal XRD analyses. Furthermore, results show that stepwise Ad addition on $Lu_3N@I_h$-C_{80} affords several Ad bis-adducts, among which two Ad bis-adducts were isolated and characterized. The X-ray structure of one bis-adduct showed clearly that the second Ad addition took place at a [6,6]-bond close to an endohedral metal atom. Theoretical calculations were also performed to rationalize the regioselectivity.

Introduction

Since the discovery of $Sc_3N@I_h$-C_{80} in 1999[1] and subsequent progress on the development of high yield synthetic methods[2] and facile isolation methods,[3] great interest has been devoted to the unique structures and favorable properties of the trimetallic nitride templated endohedral metallofullerenes (TNT-EMFs).[4] In fact, $Sc_3N@I_h$-C_{80} can be prepared in an arc reactor as the third most abundant fullerene after C_{60} and C_{70}. Nowadays, various potential applications have been proposed in organic photovoltaic (OPV) solar cells as electron acceptors or donors[5] and in biomedicine as magnetic resonance imaging (MRI) contrast agents[6] and as radiotracers.[7] For instance, Drees et al. demonstrated that the benefits of TNT-EMFs in OPVs can be attributed to their higher LUMO levels when compared to empty fullerenes such as C_{60} and C_{70}.[5] In this context, exploration of the chemical reactivity of TNT-EMFs is crucially important to establish new derivatization protocols and to develop functionalized derivatives that are suitable for applications. To date, several examples of chemical derivatization of $M_3N@I_h$-C_{80} (M = Sc, Y, Gd, Lu, etc.) have been reported, including Diels–Alder reactions,[8] Bingel–Hirsch reactions,[9] Prato reactions,[9a,10] benzyne additions,[11] reactions with diazo compounds,[12] radical additions,[13] bis-silylations,[14] silylene additions,[15] and reactions with azides.[16]

Diazirine has been recognized as an effective derivatization reagent for mono-metallic, di-metallic, and metal carbide-encaged EMFs as well as empty fullerenes.[17] Particularly, photochemical reactions of fullerenes with 2-adamantane-2,3'-[3*H*]-diazirine (**1**) allow the formation of adamantylidene (Ad) adducts.[18] At this point, incorporation of the Ad moiety to fullerenes

drastically improves their crystallinity, which enables us to conduct successful single-crystal X-ray diffraction (XRD) analyses, which are necessary to unambiguously identify the addition positions and the locations of the endohedral metal atoms.[19] In addition, the high crystallinity of such Ad adducts allows facile preparation of EMF-based crystalline nanorods that are potentially suitable for nanoscale electronics. Recently, we have found that nanorods of La@C_{2v}(9)-C_{82}(Ad) exhibit anisotropic and extremely high electron mobility whereas the drop-cast thin film of the same compound exhibited much smaller values.[18,20] Nevertheless, the chemical reactivity of TNT-EMFs with diazirine has remained unexplored. In this study, we emphasize our examination of M_3N@I_h-C_{80} (M = Sc, Lu) as the most representative TNT-EMFs. We also investigate the chemical reactivity of the minor cage isomer, Sc_3N@D_{5h}-C_{80}.[21] Because of its limited availability, only rare examples are related to derivatization of Sc_3N@D_{5h}-C_{80} and structural elucidation of its derivatives.[22] Comparison of the chemical reactivity between Sc_3N@I_h-C_{80} and Sc_3N@D_{5h}-C_{80} is expected to be valuable to enrich knowledge related to the chemical reactivity of TNT-EMFs.[23] Herein, we describe the photochemical reactions of M_3N@I_h-C_{80} (M = Sc, Lu) and Sc_3N@D_{5h}-C_{80} with **1**, and crystallographic characterization of the resulting Ad mono-adducts. Furthermore, Ad bis-addition to Lu_3N@I_h-C_{80} is investigated in this study. Few reports of the relevant literature have described bis-addition to TNT-EMFs. Few structural details of bis-adducts have been clarified.[24] We obtained a single crystal of an Ad bis-adduct of Lu_3N@I_h-C_{80}, from which details of the molecular structure were characterized using XRD.

Results and Discussion

Photochemical Reaction of TNT-EMFs with 1: Synthesis and Spectroscopic Characterization of the Ad Mono-Adducts

A summary of the photochemical reaction of TNT-EMFs with **1** is depicted in Scheme 1. A toluene solution containing Sc_3N@I_h-C_{80} and 21 equiv. of **1** was photo-irradiated using a super-high-pressure mercury-arc lamp (cutoff < 350 nm). The reaction was monitored using analytical HPLC. After irradiation for

1 h, 54% of $Sc_3N@I_h$-C_{80} was consumed and a single new peak was observed (Figure 1a). Careful analyses revealed that the single new peak included those of two products. Subsequent recycling HPLC separation afforded purification of the major product **2a** and the minor product **2b**. The conversion yields (conv.y.) of **2a** and **2b** were estimated using the HPLC peak area as 81% and 13%, respectively.

The photochemical reaction of $Lu_3N@I_h$-C_{80} and **1** was conducted under the same reaction conditions. It is noteworthy that 42 % of $Lu_3N@I_h$-C_{80} was consumed after 4 min irradiation. A single new peak was observed in the HPLC analysis (Figure 1b). Subsequent recycling HPLC separation afforded purification of the major product **3a** (conv.y. 88%, estimated using HPLC) and the minor product **3b** (conv.y. 4%, estimated using HPLC). Apparently, the reaction of $Lu_3N@I_h$-C_{80} proceeded much more rapidly than that of $Sc_3N@I_h$-C_{80} in the photolysis of **1**, suggesting that $Lu_3N@I_h$-C_{80} has a higher chemical reactivity than $Sc_3N@I_h$-C_{80}. A similar trend was also observed in silylene addition to $M_3N@I_h$-C_{80} (M = Sc, Lu).[15] In that case, silylene addition of $Sc_3N@I_h$-C_{80} proceeded much less efficiently than that of $Lu_3N@I_h$-C_{80}.

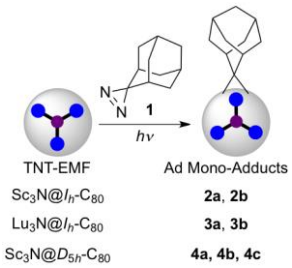

Scheme 1. Summary of the photochemical reactions of TNT-EMFs with **1**.

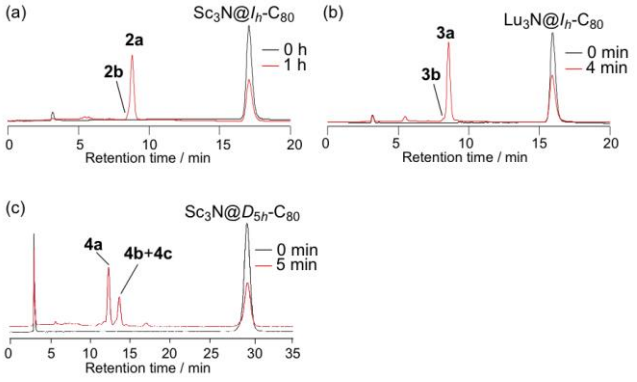

Figure 1. HPLC profiles of the reaction mixtures in the photochemical reactions of TNT-EMFs with **1**. TNT-EMF = (a) $Sc_3N@I_h$-C_{80}, (b) $Lu_3N@I_h$-C_{80}, and (c) $Sc_3N@D_{5h}$-C_{80}. Conditions: column, 5PYE (i.d. 4.6 × 250 mm); flow rate, toluene 1.0 mL min^{-1}; UV detection, 330 nm; temperature, 40°C.

Considering the addition sites, the I_h-C_{80} cage possesses two nonequivalent carbon atoms, which provide two C–C bonds. One, denoted as [6,6]-bond, is shared by two hexagonal rings. The other is shared by one hexagonal ring and one pentagonal ring and is denoted as a [5,6]-bond (see Figure 2e). In addition, two possibilities exist for the bond at the addition site, which may be cleaved or remain intact.[25] Accordingly, four addition patterns should be considered: [6,6]-open, [6,6]-closed, [5,6]-open, and [5,6]-closed structures. The ^{13}C NMR spectrum of **2a** displays two signals at 98.73 and 99.42 ppm assignable to the bonded cage carbon atoms. The chemical shifts show good agreement with the values observed for a [6,6]-open PCBM-type derivative of $Sc_3N@I_h$-C_{80} (95.55 and 96.49 ppm).[12a] Similarly, the ^{13}C NMR spectrum of **3a** displays two signals, at 98.73 and 99.42 ppm, assignable to the bonded cage carbon atoms. Consequently, results indicate that both **2a** and **3a** have [6,6]-open structures. In contrast, the ^{13}C NMR spectra of **2b** and **3b** display one signal at 91.89 and 90.02 ppm, respectively, assignable to the bonded cage carbon atom. Results show that **2a** and **3a** have [5,6]-open structures. Absorption spectra of **2a**, **2b**, **3a**, and **3b** are almost comparable to those of pristine $M_3N@I_h$-C_{80}, suggesting that these mono-adducts retain their p-electron systems and that they might have open forms rather than closed ones. In a related work, preferential [6,6]-

addition was also found for Ad addition to $La_2@I_h$-C_{80}.[25]

The photochemical reaction of $Sc_3N@D_{5h}$-C_{80} and **1** was conducted under the same protocol. After 5 min irradiation, two new peaks were observed in the analytical HPLC. The first fraction included the Ad mono-adduct **4a**. The second fraction contained two inseparable Ad mono-adducts **4b** and **4c** (Figure 1c). The conversion yields (conv.y.) of **4a** and **4b/2c** were estimated respectively using the HPLC peak area as 48% and 33%. The ratio of **4b/3c** could not be determined because NMR characterization failed as a result of the poor solubility. Nevertheless, the results show that $Sc_3N@D_{5h}$-C_{80} exhibits much higher reactivity than $Sc_3N@I_h$-C_{80} in the photolysis of **1**. Regarding this point, Dorn et al. reported that $Sc_3N@D_{5h}$-C_{80} is more reactive than $Sc_3N@I_h$-C_{80} toward 1,3-dipolar cycloaddition and Diels–Alder reactions.[22a] The chemical reactivity difference between $Sc_3N@I_h$-C_{80} and $Sc_3N@D_{5h}$-C_{80} is associated with the smaller HOMO–LUMO gap of $Sc_3N@D_{5h}$-C_{80} relative to that of $Sc_3N@I_h$-C_{80}.[23]

Regarding the D_{5h}-C_{80} cage, there are six nonequivalent carbon atoms (see Figure 3c) and nine different C–C bonds consisting of five [6,6]-bonds and four [5,6]-bonds. In terms of the combination of four adjacent rings, the nine different C–C bonds are classifiable into four groups (see Figure 3d). By considering two possibilities of whether the bond on the addition site is cleaved or not, a total of 18 addition patterns exist. The preferential formation of the three major products reflects high regioselectivity in the Ad addition to $Sc_3N@D_{5h}$-C_{80}. However, NMR spectroscopic characterization of **4a**–**4c** was prohibited because of their low solubility. Nevertheless, the similarity in their absorption spectra of **4a**–**4c** with that of $Sc_3N@D_{5h}$-C_{80} suggests that the Ad mono-adducts have open structures.

Crystallographic Characterization of the Ad Mono-Adducts

The molecular structures of 2a, 2b, 3a, and 3b were determined unambiguously using single-crystal X-ray diffraction (XRD) studies. Black crystals suitable for data collection were obtained by slow evaporation of a solution in CS_2 containing a few drops of 1,2-dichlorobenzene (1,2-DCB) for 2a, 3a, and 3b or a solution in mixed solvent of CS_2, hexane, and toluene for 2b. As presented in Figure 2, the molecular structures confirmed that 2a and

3a correspond to the [6,6]-open mono-adducts and that 2b and 3b correspond to the [5,6]-open mono-adducts, although all the outer carbon cages are also disordered except for 2b (For the minor cage orientations, see Figure S34 in Supporting Information). The opened C···C separations of the major carbon cage orientations are 2.115 Å in 2a, 2.130 Å in 2b, 2.160 Å in 3a, and 2.175 Å in 3b. It is noteworthy that such a [5,6]-open fulleroid is still rare in TNT-EMF derivatives.[12b,15,16] It is also noteworthy that the endohedral M_3N cluster is disordered. One metal site is positioned near the addition site in all cases, which is typical for EMF derivatives bearing open structures. In addition, the major orientations of the metal sites and the central nitrogen atom constitute an almost planar M_3N cluster. The X-ray structure of 2a includes 10 Sc atom sites classified into two groups. One group includes Sc1 and Sc10 near the addition site, with their occupancies summed to 1.00. The other group consists of eight Sc sites (Sc2–Sc9) with their occupancies summed to 2.00. In the X-ray structure of 2b, five Sc atom sites were assigned, and were classified into two groups. Sc1 is ordered with 1.00 occupancy and points toward the addition site. The other group consists of four Sc atom sites, of which Sc2 and Sc4 have their occupancies summed to 1.00 (Sc2/Sc4 = 0.57/0.43), with Sc3 and Sc5 having their occupancies summed to 1.00 (Sc3/Sc5 = 0.57/0.43). The X-ray structure of 3a has nine Lu atom sites divided into three parts. One part includes only Lu1 with 1.00 occupancy and points to the addition site. The other eight Lu sites occur in two more parts. Their occupancies were 0.28 for Lu2, Lu3, Lu6, and Lu7, and 0.22 for Lu4, Lu5, Lu8, and Lu9. In the X-ray structure of 3b, there are 14 Lu atom sites; those were divided into two parts. One part includes only Lu1 with 1.00 occupancy, which points to the addition site. The other 12 Lu atom sites have their occupancies summed to 2.00.

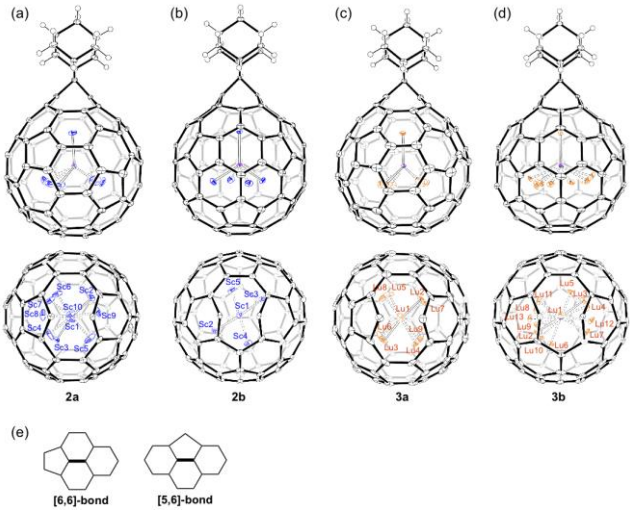

Figure 2. Thermal ellipsoid plots of (a) **2a** ([6,6]-open Ad mono-adduct), (b) **2b** ([5,6]-open Ad mono-adduct), (c) **3a** ([6,6]-open Ad mono-adduct), and (d) **3b** ([5,6]-open Ad mono-adduct) with thermal ellipsoids shown at the 50% probability level for 90 K: (a) front view, (b) top view (Ad moieties are omitted for clarity). Only the major cage orientation (occupancies of the major cages: **2a**, 0.45; **3a**, 0.50; **3b**, 0.85) is shown except for **2b**. Occupancies of these metal (Sc or Lu) sites in **2a**, **2b**, **3a**, and **3b** are the following. **2a**: Sc1, 0.67; Sc2, 0.42; Sc3, 0.25; Sc4, 0.17; Sc5, 0.37; Sc6, 0.29; Sc7, 0.08; Sc8, 0.21. **2b**: Sc1, 1.00; Sc2, 0.57; Sc3, 0.57; Sc4, 0.43; Sc5, 0.43. **3a**: Lu1, 1.00; Lu2, 0.28; Lu3, 0.28; Lu4, 0.22; Lu5, 0.22; Lu6, 0.28; Lu7, 0.28; Lu8, 0.22; Lu9, 0.22. **3b**: Lu1, 1.00; Lu2, 0.62; Lu3, 0.49; Lu4, 0.23; Lu5, 0.12; Lu6, 0.12; Lu7, 0.12; Lu8, 0.10; Lu9, 0.07; Lu10, 0.05; Lu11, 0.03; Lu12, 0.02; Lu13, 0.01, Lu14, 0.02 (not shown). Solvate molecules are omitted for clarity. (e) Two different bonds on I_h-C_{80}.

The molecular structures of the $Sc_3N@D_{5h}$-C_{80} adducts **4a**–**4c** were also characterized by single-crystal XRD studies. Black crystals of **4a** and the mixture of **4b/4c** suitable for data collection were obtained through slow evaporation of a solution in CS_2 containing a few drops of 1,2-DCB. The X-ray structures of **4b** and **4c** were obtained from the mixed crystal, in which the structure of **4b** is related to the major site with 0.89 occupancy and that of **4c** is related to the minor site with 0.11 occupancy. The X-ray structures

presented in Figure 3 reveal that **4a** derives from addition at the [6,6]-(b–c) bond, **4b** results from addition at the [6,6]-(a–b) bond, and **4c** results from addition at the [6,6]-(d–f) bond, accompanied in each case by C–C bond cleavage. The opened C···C separations of the major carbon cage orientations are: 2.051 Å in **4a**, 2.153Å in **4b**, and 2.153Å in **4c**. For the minor cage orientations of **4a**, see Figure S33 in Supporting Information. As shown in the X-ray structures of **2a**, **2b**, **3a**, and **3b**, the endohedral M_3N clusters are also disordered in **4a**–**4c**. One metal site is positioned near the addition site. In addition, the major orientations of the metal sites and the central nitrogen atom constitute an almost planar M_3N cluster. In a related work, Echegoyen et al. reported the synthesis of five PCBM derivatives of $Sc_3N@D_{5h}$-C_{80} by the reaction with the *p*-toluenesulfonyl tosyl hydrazone of phenyl butyric acid methyl ester and the X-ray structure of one of the derivatives, in which the addition occurred at the [6,6]-(f–f) bond.[22b] At this point, the regioselectivity in the photochemical reaction of $Sc_3N@D_{5h}$-C_{80} with **1** differs from the reaction with the hydrazone. In contrast, the addition of a $W(CO)_3(Ph_2PCH_2CH_2PPh_2)$ group to $Sc_3N@D_{5h}$-C_{80} occurs at a [6,6]-(b–c) bond and leaves the C–C bond intact.[26] The 1,3-dipolar cycloaddition of *N*-tritylazomethine ylide to $Sc_3N@D_{5h}$-C_{80} produced two mono adducts, which were assigned as additions to [6,6]-bonds on the basis of NMR measurements.[22a] Subsequent, re-examination of this addition through computational studies suggested that the additions occur over [5,6]-bonds.[27] Crystallographic studies are needed to fully establish the addition site in this cycloaddition reaction.

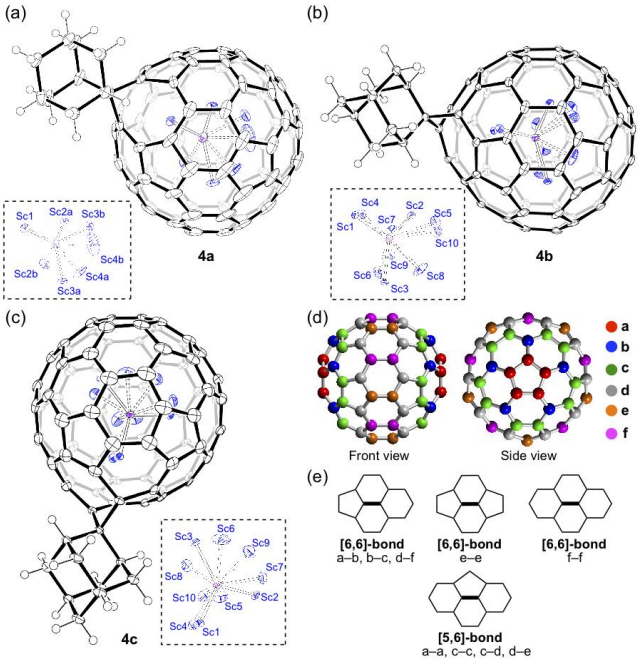

Figure 3. Thermal ellipsoid plots of (a) **4a** ([6,6]-(b–c)-open Ad mono-adduct), (b) **4b** ([6,6]-(a–b)-open Ad mono-adduct), and (c) **4c** ([6,6]-(d–f)-open Ad mono-adduct) with thermal ellipsoids shown at the 50% probability level for 90 K. Only the major cage orientation (occupancy = 0.46) is shown in **4a**. The crystal structure of **4b**/**4c** comprises **4b** with 0.89 site occupancy and **4c** with 0.11 site occupancy. Solvate molecules are omitted for clarity. Numbering of the disordered Sc atoms is presented in the inset. Occupancies of these Sc sites in **4a** and **4b**/**4c** are the following. **4a**: Sc1, 1.00; Sc2A, 0.56; Sc3A, 0.43; Sc4A, 0.13; Sc2B, 0.44; Sc3B, 0.31; Sc4B, 0.13. **4b**/**4c**: Sc1, 0.91; Sc2, 0.76; Sc3, 0.76; Sc4, 0.09; Sc5, 0.09; Sc6, 0.09; Sc7, 0.08; Sc8, 0.08; Sc9, 0.07; Sc10, 0.07. (d) Front and side views of D_{5h}-C_{80}. Five nonequivalent carbon atoms a, b, c, d, e, and f are colored, respectively, as red, blue, green, gray, orange, and pink. (e) Nine bonds on D_{5h}-C_{80}.

Theoretical Calculations for $M_3N@C_{80}$(Ad) (M = Sc, Lu)

Geometry optimizations of the [6,6]-open and [5,6]-open structures for the Ad mono-adducts of $Sc_3N@I_h$-C_{80} were conducted to assess their relative energies, as presented in Figure 4. The results show that the [6,6]-open structure is more stable than the [5,6]-open structure. The [5,6]-open structure, which corresponds to 2b, is 2.74 kcal mol^{-1} higher in energy than the [6,6]-open

structure that corresponds to 2a. In the optimized structures, one Sc atom is located near the site of addition, as found in the X-ray structures. Based on the thermodynamic perspective, it is reasonable that the [6,6]-open $Sc_3N@I_h$-C_{80}(Ad) is the major product and the [5,6]-open $Sc_3N@I_h$-C_{80}(Ad) is the minor product. Such is also the case with $Lu_3N@I_h$-C_{80}(Ad). DFT calculations for the [6,6]-open and the [5,6]-open structures of $Lu_3N@I_h$-C_{80}(Ad) reveal that the [6,6]-open structure (3a) is more stable than the [5,6]-open structure (3b) by 5.16 kcal mol^{-1}. It is noteworthy that the [6,6]-closed form of $Sc_3N@I_h$-C_{80}(Ad) has no energy minimum - attempts to optimize the [6,6]-closed structure led to a [6,6]-open structure.

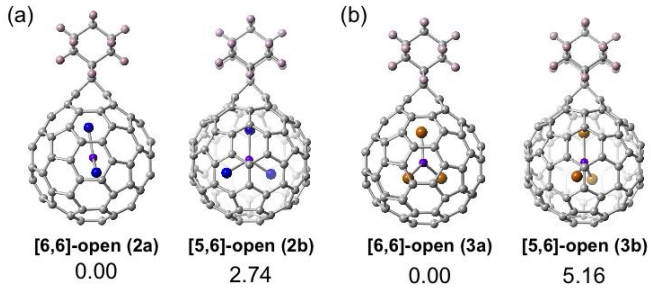

Figure 4. Optimized structures and their relative energies (in kcal mol^{-1}) of the [6,6]-open and [5,6]-open isomers of (a) $Sc_3N@I_h$-C_{80}(Ad) and (b) $Lu_3N@I_h$-C_{80}(Ad) calculated at the B3LYP/6-31G(d)~SDD level.

In $M_3N@C_{80}$ (M = Sc, Lu), NMR spectroscopic experiments and DFT calculations show that the encaged M_3N cluster can rotate in the cage interior.[1,21,28] To assess the possibility in the rotation of the M_3N cluster in the Ad mono-adducts, the relative energies of [6,6]-open and [5,6]-open $M_3N@I_h$-C_{80}(Ad) (M = Sc, Lu) structures were calculated by changing the M_3N orientation. As presented in Figure 5, the relative energies fall in a narrow range as narrow as < 3 kcal mol^{-1} in all cases. Therefore, it is reasonable to consider that the M_3N cluster is allowed to rotate like a spinning top in **2a**, **2b**, **3a**, and **3b**, as proposed in a Bingel–Hirsch derivative of $Y_3N@I_h$-C_{80}.[9b]

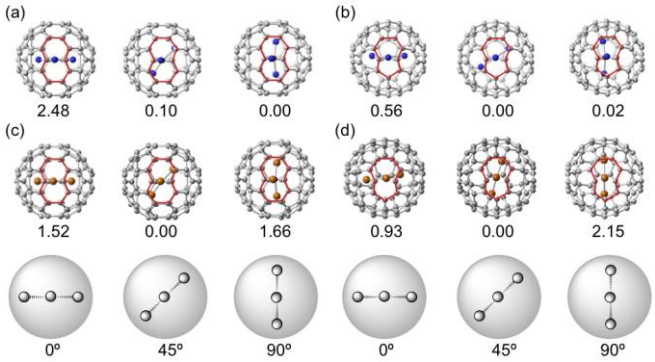

Figure 5. (a–d) Optimized structures (top views) and their relative energies (in kcal mol^{-1}) of the Ad mono-adducts by changing the M_3N cluster orientation calculated at the B3LYP/6-31G(d)~SDD level. (a) [6,6]-open $Sc_3N@I_h$-C_{80}(Ad), (b) [5,6]-open $Sc_3N@I_h$-C_{80}(Ad), (c) [6,6]-open $Lu_3N@I_h$-C_{80}(Ad), and (d) [5,6]-open $Lu_3N@I_h$-C_{80}(Ad). Ad moieties are omitted for clarity. Schematic representation of the initial orientation of the M_3N cluster for geometry optimization is shown in the bottom; the rotation angle = 0°, 45° , or 90°.

Geometry optimization of five selected [6,6]-adducts of $Sc_3N@D_{5h}$-C_{80}, as [6,6]-(a–b)-open, [6,6]-(b–c)-open, [6,6]-(d–f)-open, [6,6]-(e–e)-open, and [6,6]-(e–e)-closed $Sc_3N@D_{5h}$-C_{80}(Ad), were also conducted based on the fact that Ad addition prefers [6,6]-bonds to [5,6]-bonds in $Sc_3N@I_h$-C_{80} as described above. The optimized structures and the relative energies are presented in Figure 6. The results show that the energy difference between the [6,6]-(b–c)-open structure corresponding to **4a** and the [6,6]-(a–b)-open structure corresponding to **4b** is small and the latter is 0.40 kcal mol^{-1} higher in energy than the former. The [6,6]-(d–f)-open structure corresponding to **4c** is energetically the most stable isomer among the five isomers. Accordingly, it is reasonable to consider that thermodynamically stable, Ad mono-adducts were obtained in the experiments.

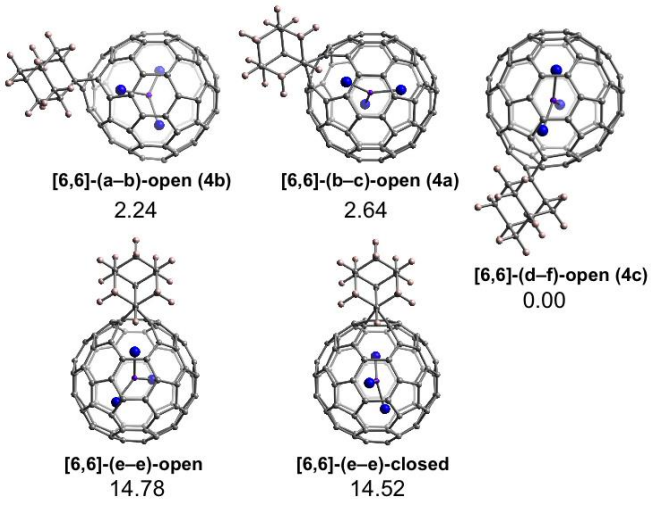

Figure 6. Optimized structures and the relative energies (in kcal mol^{-1}) of five selected isomers of $Sc_3N@D_{5h}$-C_{80}(Ad) calculated at the B3LYP/6-31G(d)~SDD level.

Synthesis and Characterization of Ad Bis-Adducts of $Lu_3N@I_h$-C_{80}

Encouraged by the high chemical reactivity of $Lu_3N@I_h$-C_{80}, additional Ad addition to **3a** was conducted for the synthesis of Ad bis-adducts (Scheme 2). A toluene solution containing **3a** and 200 equiv of **1** was photo-irradiated using a super-high-pressure mercury-arc lamp (cutoff < 350 nm). The reaction was monitored using analytical HPLC. After irradiation for 5 min, 64% of **3a** was consumed and new products were formed (Figure 7). The conversion yields of the bis-adducts were estimated as 70% using the HPLC peak area. Subsequent HPLC separation using a Buckyprep column for the first step followed by recycling HPLC separation using a 5NPE column for the second step afforded purification of two Ad bis-adduct isomers **5a** and **5b**, but the amounts of the isolated samples were very small. The absorption spectra of **5a** and **5b** resemble those of **3a**, suggesting that the second Ad addition also led to formation of an open structure. Although the ^{1}H NMR spectra of **5a** and **5b** provided no meaningful information related to structural elucidation, the molecular structure of **5b** was characterized using single-crystal XRD, as shown in Figure 8. The crystals belong to the monoclinic space group *P*2/*n*. The X-ray structure reveals that **5b** results from addition at the [6,6]-(34–55)

bond (for the numbering of carbon atoms, see Figure 9b) that are close to an encaged Lu atom with C–C bond cleavage. The two opened C···C separations are 2.158 and 2.165 Å.

Charge densities and pyramidalization angles, defined as the p orbital axis vector (POAV)[29] of the individual carbon atom, are often used as a powerful criterion to assign the addition sites. It is noteworthy that these values are strongly dependent on the orientation of the encaged M_3N cluster in TNT-EMFs. In pristine $M_3N@I_h$-C_{80} and $M_3N@D_{5h}$-C_{80} (M = Sc, Lu), the existence of the random rotation of the M_3N cluster prevents us from applying the charge densities and POAV values at each carbon atom to assign reactive sites. However, the rotation of the Lu_3N cluster in **3a** is rather more restricted than that in pristine $Lu_3N@I_h$-C_{80}, as indicated in the X-ray structure. Encouraged by that fact, we examined the POAV values and charge densities of the individual carbon atom in **3a**, as presented in Table 1. The DFT calculations reveal that the negative charge density is localized at carbon atoms close to the encaged Lu atoms, such as C(10), C(12), C(34), C(57), and C(68). Among them, it is reasonable to consider that carbon atoms C(10) and C(12) are much less reactive because of the severe steric congestion. In terms of the POAV criterion, carbon atoms C(36), C(57), and C(67), which are close to the encaged Lu atoms as well, tend to have large POAV values. In this respect, it is reasonable to consider that the reaction site of the second Ad addition in **3a** is also governed by the localization of the encaged Lu atoms. Evidently, the regioselectivity in the Ad bis-addition is regulated by the triangular structure of the endohedral Lu_3N cluster as shown in Figure 8. In related works, crystallographic characterization of Ad bis-adducts of $La_2@I_h$-C_{80} and $La_2@D_2$-C_{72} also revealed that the second Ad additions occurred at sites near the encaged La atoms.[30,31] Figure 9 presents the optimized structures and their relative energies of five selected isomers of $Lu_3N@I_h$-$C_{80}(Ad)_2$. The Ad bis-adduct with the second addition at [6,6]-(34–55) site (designated as [6,6]-(34–55) bis-adduct), which agrees with the X-ray structure of **5b**, is energetically the most stable among the five candidates. The [6,6]-(36–57) and [6,6]-(35–36) bis-adducts, in which the second addition site is near one of the encaged Lu atoms, are 1.36 and 3.76 kcal mol^{-1}, respectively, higher in energy than

the [6,6]-(34–35) bis-adduct. However, second addition at C–C bonds far from the encaged Lu atom leads to energetically less stable products such as [5,6]-(32–33) and [6,6]-(30–31) bis-adducts, which are 24.10 and 23.00 kcal mol^{-1}, respectively, higher in energy than [6,6]-(34–55) bis-adduct.

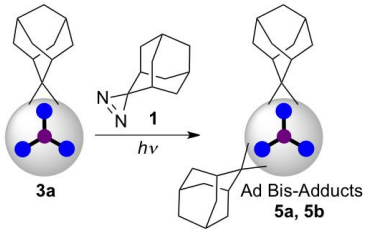

Scheme 2. Photochemical reaction of **3a** with diazirine **1**.

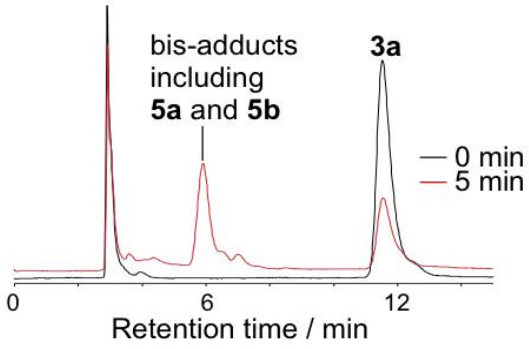

Figure 7. HPLC profiles of the reaction mixture (red line, before photo-irradiation; black line, photo-irradiation for 5 min) in photochemical reactions of **3a** with **1**. Conditions: column, Buckyprep (i□□□□4.6 × 250 mm); flow rate, toluene 1.0 mL min^{-1}; UV detection, 330 nm; temperature, 40 °C.

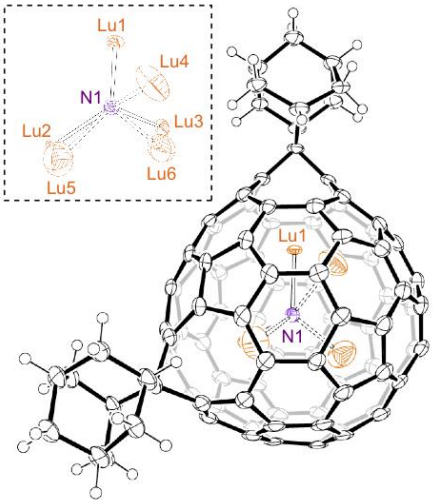

Figure 8. ORTEP plots of the asymmetric unit of **5b** with thermal ellipsoids shown at the 50% probability level for 90 K. Solvate molecules are omitted for clarity. Numbering of the disordered Lu atoms is presented in the inset.

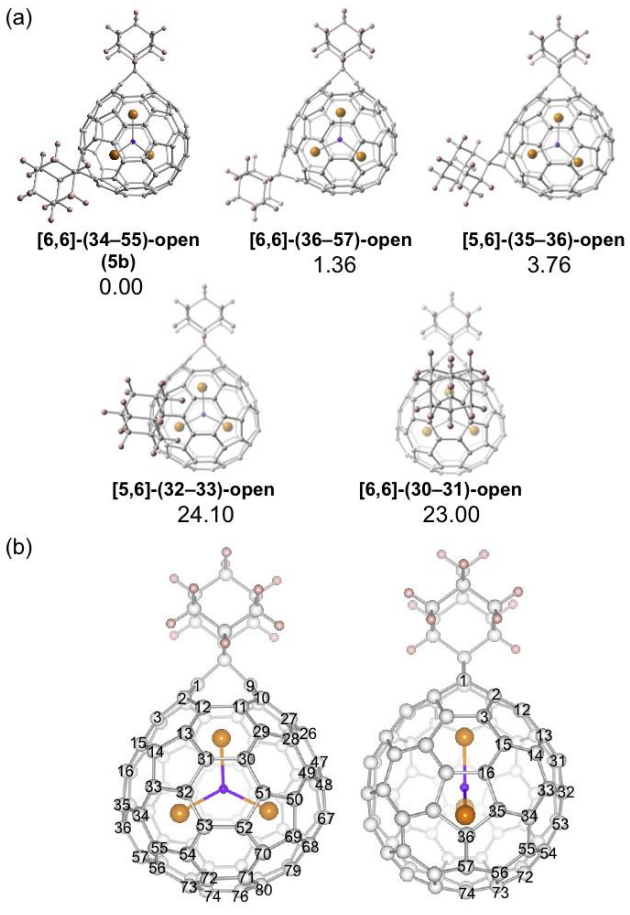

Figure 9. (a) Optimized structures and their relative energies (in kcal mol^{-1}) of five selected isomers of $Lu_3N@D_{5h}$-$C_{80}(Ad)_2$, in which the labeling shows the second addition sites calculated at the B3LYP/6-31G~SDD level. (b) Selected carbon atoms in two orthogonal views of **3a** are numbered according to IUPAC recommendations.[32]

Table 1. Mulliken Charge Densities and POAV Values[a] of Carbon Atoms in [6,6]-Open $Lu_3N@I_h$-C_{80}(Ad) Calculated at the B3LYP/3-31G~SDD Level.

Carbon atom	Mulliken charge density	POAV value	Carbon atom	Mulliken charge density	POAV value
C(1)	–0.1333	4.08	C(47)	–0.0874	8.82
C(2)	–0.1852	10.53	C(48)	–0.1448	9.50
C(3)	–0.0998	7.56	C(49)	–0.1119	8.75
C(9)	–0.1359	5.67	C(50)	–0.0426	10.46
C(10)	–0.2535	7.56	C(51)	–0.0098	10.81
C(11)	–0.1660	9.61	C(52)	–0.0049	10.55
C(12)	–0.2532	8.36	C(53)	–0.0476	8.88
C(13)	–0.0323	9.40	C(54)	–0.0354	10.33
C(14)	–0.0303	11.19	C(55)	–0.1017	9.93
C(15)	–0.0802	8.67	C(56)	–0.1812	9.42
C(16)	–0.1055	8.88	C(57)	–0.2061	12.10
C(26)	–0.0953	9.47	C(67)	–0.1592	13.08
C(27)	–0.0681	9.13	C(68)	–0.2294	10.30
C(28)	–0.0069	10.02	C(69)	–0.1022	9.15
C(29)	–0.0428	9.32	C(70)	–0.0269	10.20
C(30)	–0.0428	8.65	C(71)	–0.0734	8.97
C(31)	–0.0010	9.96	C(72)	–0.0175	10.53
C(32)	–0.0047	10.22	C(73)	–0.0647	10.07
C(33)	–0.0352	10.45	C(74)	–0.0964	8.80
C(34)	–0.1817	8.72	C(76)	–0.0210	10.32
C(35)	–0.1651	11.16	C(79)	–0.1656	10.27

C(36)	–0.1591	13.67	C(80)	–0.0664	9.87

[a] Both terms calculated in the B3LYP/6-31G(d)~SDD optimized structures (charges with B3LYP/3-21G~SDD).

Electrochemical Properties

The redox potentials of the Ad adducts measured using differential pulse voltammetry (DPV) are presented in Table 2 together with the calculated HOMO/LUMO levels. The first oxidation potentials of the Ad mono-adducts were shifted cathodically by 10–110 mV. The first reduction potentials were also shifted cathodically by 10–130 mV, relative to those of the corresponding pristine $M_3N@C_{80}$. The trend accords well with the redox properties of other Ad adducts of EMFs reported previously. In addition, the redox properties agree well with the calculated HOMO/LUMO levels. It is noteworthy that the first reduction potential of 3b is comparable to that of a $Lu_3N@I_h$-C_{80}PCBH analogue (–1.51 V vs. Fc/Fc^+); that of 3a is even higher.[5] In 5a and 5b, a further cathodic shift is evident.

Table 2. Redox Potentials[a] and HOMO/LUMO Levels of $M_3N@C_{80}$ and Their Ad Adducts

Compound	$^{ox}E_1$	$^{red}E_1$	$^{red}E_2$	$^{red}E_3$	HOMO[c]	LUMO[c]
$Sc_3N@I_h$-C_{80}[b]	+0.65	–1.07	–1.46	–1.78	–5.51	–2.97
2a[b]	+0.58	–1.15	–1.59	–1.89	–5.38	–2.98
2b[b]	+0.57	–1.08			–5.38	–3.04
$Lu_3N@I_h$-C_{80}	+0.61	–1.41	–1.91	–2.56	–5.48	–2.90
3a	+0.50	–1.57	–2.08	–2.73	–5.28	–2.69
3b	+0.52	–1.48	–2.15		–5.30	–2.65
5a	+0.40	–1.69	–2.26			
5b	+0.42	–1.62			–5.16	–2.55
$Sc_3N@D_{5h}$-C_{80}	+0.29	–1.36	–1.78	–2.31	–5.35	–3.05
4a	+0.28	–1.44	–1.91	–2.50	-5.11	–2.77
4b/**4c**	+0.20	–1.38	–1.90	–2.50	–4.98	–2.77

[a] Values given as V vs. Fc/Fc^+ and were obtained using differential pulse voltammetry (DPV). [b] Benzonitrile was used as the solvent instead of 1,2-DCB because of the low solubility. [c] Calculated at the B3LYP/6-31G(d)~SDD level.

Conclusions

We successfully synthesized and characterized not only the [6,6]-open Ad mono-adducts but also the [5,6]-open Ad mono-adducts of $M_3N@I_h$-C_{80} (M = Sc, Lu) by the photochemical reaction with diazirine 1. Preferential formation of the [6,6]-open Ad mono-adducts rather than the [5,6]-open Ad mono-adducts can be rationalized by the difference in thermodynamic stability. We noted the higher reactivity of $Lu_3N@I_h$-C_{80} than $Sc_3N@I_h$-C_{80}. Additionally, we synthesized and characterized three major isomers of Ad mono-adducts of $Sc_3N@D_{5h}$-C_{80} using the photochemical reaction with diazirine **1**. Single-crystal XRD analyses showed that the major mono-adducts correspond to [6,6]-(b–c)-open, [6,6]-(a–b)-open, and [6,6]-(d–f)-open Ad mono-adducts. Furthermore, we have synthesized and characterized two Ad bis-adducts of $Lu_3N@I_h$-C_{80} by stepwise Ad addition. Single-crystal XRD analysis of one bis-adduct showed that the second Ad addition took place at [6,6]-(34–55)-bond close to an endohedral metal atom. These results clearly demonstrate that the addition sites for multiple additions can be governed by the orientation of the endohedral trimetallic nitride cluster. Further studies will be devoted to regioselective tris-addition on $M_3N@C_{80}$ by taking advantage of the trianglar structure of the endohedral M_3N cluster.

Experimental Section

General Procedure for the Photochemical Reaction of TNT-EMF ($Sc_3N@I_h$-C_{80}, $Lu_3N@I_h$-C_{80}, and $Sc_3N@D_{5h}$-C_{80}) with 1. A 10 mL aliquot of a toluene solution of TNT-EMF (9.0×10^{-5} M) and 21 equiv. of **1** (310 mg, 1.9×10^{-3} M) were placed in a Pyrex tube. After degassing using three freeze–pump–thaw cycles under reduced pressures, the mixture was irradiated with a high-pressure mercury lamp through a cutoff filter (cutoff < 350 nm) under argon atmosphere. The residue was subsequently purified using preparative high-performance column chromatography (HPLC) with a 5PYE column (20 mm × 250 mm i.d., Nacalai Tesque Inc.; eluent, toluene) to afford the corresponding Ad mono-adducts.

Synthesis of Ad Mono-adducts of $Sc_3N@I_h$-C_{80}. In the reaction of $Sc_3N@I_h$-C_{80} with **1**, two Ad mono-adducts, designated as **2a** as the major isomer and **2b** as the minor isomer, were prepared and isolated according to general procedures using $Sc_3N@I_h$-C_{80} (1.0 mg, 9.0×10^{-5} M) upon photo-irradiation for 1 h.

Conversion yields were 81% (**2a**) and 13% (**2b**) (determined using the HPLC peak area).

Spectral Data for 2a. ^{1}H NMR (500 MHz, CS_2 (C_6D_6 in capillary), 293 K) δ = 3.05 (s, 2H), 2.86 (d, J = 12.0 Hz, 2H), 2.77 (d, J = 12.5 Hz, 2H), 2.56 (s, 1H), 2.49 (d, J = 13.0 Hz, 2H), 2.44 (d, J = 10.0 Hz, 2H), 2.40 (s, 1H), 2.37 (s, 2H) ppm; ^{13}C NMR (125 MHz, CS_2 (C_6D_6 in capillary for the measurement in the aromatic region and $(CD_3)_2CO$ in capillary for the measurement in the aliphatic region), 293 K) δ = 154.07, 153.15, 151.86, 151.73, 150.76, 149.37, 147.87, 147.78, 147.58, 146.02, 145.97, 145.84, 145.60, 145.03, 144.95, 144.72, 144.31, 143.83, 143.75, 142.93, 142.52, 142.50, 142.26, 142.18, 141.65, 141.11, 140.53, 140.48, 140.11, 139.79, 139.77, 138.59, 136.64, 136.33, 136.21, 136.19, 135.84, 135.34, 129.65, 129.16, 124.18, 123.60, 99.42, 98.73, 47□□□, 38.08, 35.13, 34.94, 33.96, 28.74, 28.22 ppm; MALDI-TOF MS (matrix = 1,1,4,4-tetraphenyl-1,3-butadiene) m/z 1243 ([M]$^-$), 1109 ([M – Ad]$^-$).

Crystal Data for 2a. $Sc_3NC_{90}H_{14}\cdot 0.82(C_6H_4Cl_2)\cdot 0.86(CS_2)$, M_w = 1430.15, crystal size: 0.53 × 0.38 × 0.35 mm, triclinic, $P\bar{1}$, a = 11.158(2) Å, b = 14.563(3) Å, c = 16.418(3) Å, α = 89.100(2)°, β = 75.785(2)°, γ = 74.130(2)°, V = 2483.8(9) Å^3, Z = 2, D_{calc} = 1.912 g/cm^3, μ = 0.631 mm^{-1}, T = 90 K, 64324 reflections, 23511 unique reflections; 18837 with $I > 2\sigma(I)$; R_1 = 0.0656 [$I > 2\sigma(I)$], wR_2 = 0.1797 (all data), GOF (on F^2) = 1.027. The maximum residual electron density is equal to 1.14 e Å^{-3}.

Spectral Data for 2b. ^{1}H NMR (500 MHz, CS_2 (C_6D_6 in capillary), 293 K) δ = 3.42 (s, 1H), 3.00 (d, J = 12.0 Hz, 2H), 2.57 (d, J = 12.5 Hz, 2H), 2.50 (s, 2H), 2.48 (d, J = 12.0 Hz, 2H), 2.30 (d, J = 12.0 Hz, 2H), 2.21 (d, J = 13.0 Hz, 2H), 1.80 (s, 1H) ppm; ^{13}C NMR (125 MHz, CS_2 (C_6D_6 in capillary), 293 K) δ = 154.19, 150.38, 149.57, 148.99, 147.56, 147.46, 147.22, 147.01, 146.92, 146.34, 146.26, 144.97, 144.89, 144.76, 144.52, 144.15, 143.13, 142.58, 142.55, 142.48, 142.32, 141.68, 141.25, 141.14, 141.08, 140.92, 140.26, 139.99, 139.57, 137.99, 137.75, 137.61, 136.42, 136.19, 135.92, 135.70, 133.38, 132.17, 125.87, 125.35, 118.37, 91.89, 43.31, 37.94, 35.14, 32.99, 29.93, 28.54 ppm; MALDI-TOF MS (matrix = 1,1,4,4-tetraphenyl-1,3-butadiene) m/z 1243 ([M]$^-$).

Crystal Data for 2b. $Sc_3NC_{90}H_{14}\cdot 0.50(CS_2)$, M_w = 1281.97, crystal size: 0.14 × 0.10 × 0.06 mm, monoclinic, $C2/c$, a = 18.857(7) Å, b = 11.500(4) Å, c =

40.438(15) Å, β = 92.732(5)°, V = 8759(6) Å^3, Z = 8, D_{calc} = 1.944 g/cm^3, μ = 0.574 mm^{-1}, T = 90 K, 20686 reflections, 8827 unique reflections; 7014 with $I > 2\sigma(I)$; R_1 = 0.0610 [$I > 2\sigma(I)$], wR_2 = 0.1470 (all data), GOF (on F^2) = 1.074. The maximum residual electron density is equal to 0.45 e Å^{-3}.

Synthesis of Ad Mono-adducts of $Lu_3N@I_h$-C_{80}. In the reaction of $Lu_3N@I_h$-C_{80} with **1**, two Ad mono-adducts, designated as **3a** as the major isomer and **3b** as the minor isomer, were prepared and isolated according to the general procedure using $Lu_3N@I_h$-C_{80} (1.4 mg, 9.0×10^{-5} M) upon photo-irradiation for 4 min. Conversion yields: 88% (**3a**) and 4% (**3b**) (determined using the HPLC peak area).

Spectral Data for 3a. ^{1}H NMR (500 MHz, CS_2 (C_6D_6 in capillary), 293 K) δ = 3.19 (s, 2H), 2.95 (d, J = 13.0 Hz, 2H), 2.89 (d, J = 13.0 Hz, 2H), 2.57 (s, 1H), 2.51 (s, 1H), 2.46 (d, J = 13.0 Hz, 2H), 2.42 (d, J = 13.0 Hz, 2H), 2.38 (s, 2H) ppm; ^{13}C NMR (125 MHz, CS_2 ($(CD_3)_2CO$ in capillary), 293 K) δ = 152.49, 151.41, 149.63, 148.92, 148.87, 148.82, 147.62, 146.98, 146.36, 146.16, 146.02, 145.83, 145.46, 145.16, 145.03, 144.50, 144.45, 144.05, 143.84, 143.74, 143.43, 143.28, 143.17, 142.90, 142.59, 141.72, 141.66, 140.90, 140.58, 140.27, 139.07, 136.66, 136.50, 136.27, 136.14, 135.92, 135.64, 129.59, 129.49, 128.30, 125.45, 125.41, 100.59, 98.30, 49.69, 39.10, 35.54, 35.42, 34.88, 29.40, 28.87 ppm; MALDI-TOF MS (matrix = 1,1,4,4-tetraphenyl-1,3-butadiene) m/z 1633 ([M]$^-$).

Crystal Data for 3a. $Lu_3NC_{90}H_{14} \cdot 0.82(C_6H_4Cl_2) \cdot 0.86(CS_2)$, M_w = 1810.68, crystal size: 0.328 × 0.211 × 0.158 mm, triclinic, $P\bar{1}$, a = 11.1632(3) Å, b = 14.6181(4) Å, c = 16.4080(4) Å, α = 88.8950(10)°, β = 75.5140(10)°, γ = 74.4890(10)°, V = 2494.74(11) Å^3, Z = 2, D_{calc} = 2.410 g/cm^3, μ = 6.111 mm^{-1}, T = 90 K, 63208 reflections, 21628 unique reflections; 20198 with $I > 2\sigma(I)$; R_1 = 0.0509 [$I > 2\sigma(I)$], wR_2 = 0.1211 (all data), GOF (on F^2) = 1.236. The maximum residual electron density is equal to 5.304 e Å^{-3}.

Spectral Data for 3b. ^{1}H NMR (500 MHz, CS_2 (C_6D_6 in capillary), 293 K) δ = 3.52 (s, 1H), 3.13 (d, J = 12.5 Hz, 2H), 2.70 (d, J = 13.0 Hz, 2H), 2.55 (s, 2H), 2.50 (d, J = 13.0 Hz, 2H), 2.34 (d, J = 13.0 Hz, 1H), 2.33 (d, J = 13.0 Hz, 1H), 2.25 (d, J = 13.0 Hz, 2H), 2.04 (s, 1H) ppm; ^{13}C NMR (125 MHz, CS_2 (benzene-d_6 in capillary), 293 K) δ = 150.14, 149.44, 148.45, 148.16, 147.47, 146.01, 145.88, 145.71, 145.44, 145.31, 144.96, 144.59, 144.06, 143.86, 143.58, 143.54,

143.35, 143.15, 142.48, 142.35, 141.68, 141.63, 141.47, 141.14, 140.65, 140.40, 139.62, 138.70, 138.47, 138.40, 136.95, 136.88, 135.61, 133.34, 132.58, 131.23, 128.95, 126.66, 120.33, 91.29, 45.00, 38.42, 35.10, 35.05, 33.51, 30.13, 28.75 ppm; MALDI-TOF MS (matrix = 1,1,4,4-tetraphenyl-1,3-butadiene) *m/z* 1633 ([*M*]$^-$).

Crystal Data for 3b. $Lu_3NC_{90}H_{14}\cdot 0.92(C_6H_4Cl_2)\cdot 0.058(CS_2)$, M_w = 1813.32, crystal size: 0.285 × 0.172 × 0.136 mm, triclinic, *P*–1, a = 11.1760(5) Å, b = 14.8131(7) Å, c = 16.2019(9) Å, α = 88.358(2)°, β = 75.314(2)°, γ = 74.317(2)°, V = 2495.7(2) Å^3, Z = 2, D_{calc} = 2.413 g/cm^3, μ = 6.106 mm^{-1}, T = 90 K, 68769 reflections, 23644 unique reflections; 21820 with $I > 2\sigma(I)$; R_1 = 0.0505 [$I > 2\sigma(I)$], wR_2 = 0.1190 (all data), GOF (on F^2) = 1.252. The maximum residual electron density is equal to 2.75 e Å^{-3}.

Synthesis of Ad Mono-adducts of $Sc_3N@D_{5h}$-C_{80}. The photochemical reaction of $Sc_3N@D_{5h}$-C_{80} with **1** was conducted according to the general procedure using $Sc_3N@D_{5h}$-C_{80} (1.0 mg, 9.0 × 10^{-5} M) upon photo-irradiation for 6 min. Conversion yields: 48% (**4a**) and 33% (**4b**+**4c**) (determined using HPLC peak area). Two main fractions were separated from the reaction mixture by preparative HPLC. The first fraction includes Ad mono-adduct **4a**. The second fraction includes two inseparable Ad mono-adducts **4b** and **4c** as the major products.

Spectral Data for 4a. ^{1}H NMR (500 MHz, CS_2 (C_6D_6 in capillary), 293 K) δ = 3.11 (s, 1H), 2.88 (d, J = 11.0 Hz, 1H), 2.85 (d, J = 10.5 Hz, 1H), 2.77 (d, J = 12.5 Hz, 1H), 2.58 (d, J = 11.0 Hz, 1H), 2.53 (s, 1H), 2.47–2.30 (m, 7H), 2.13 (d, J = 13.0 Hz, 1H) ppm; ^{13}C NMR (125 MHz, CS_2 (C_6D_6 in capillary), 293 K): not obtained because of the low solubility; MALDI-TOF MS (matrix = 1,1,4,4-tetraphenyl-1,3-butadiene) *m/z* 1243 ([*M*]$^-$).

Crystal Data for 4a. $Sc_3NC_{90}H_{14}\cdot 0.63(C_6H_4Cl_2)\cdot 1.24(CS_2)$, M_w = 1.430.91, crystal size: 0.251 × 0.122 × 0.063 mm, triclinic, *P*–1, a = 11.153(2) Å, b = 14.597(3) Å, c = 16.334(3) Å, α = 88.78(3)°, β = 75.82 (3)°, γ = 74.50(3)°, V = 2481.7(10) Å^3, Z = 2, D_{calc} = 1.914 g/cm^3, μ = 0.643 mm^{-1}, T = 90 K, 33046 reflections, 13153 unique reflections; 10922 with $I > 2\sigma(I)$; R_1 = 0.0845 [$I > 2\sigma(I)$], wR_2 = 0.2176 (all data), GOF (on F^2) = 1.092. The maximum residual electron density is equal to 1.71 e Å^{-3}.

Spectral Data for 4b/4c. ^{1}H NMR (500 MHz, CS_2 (C_6D_6 in capillary), 293 K) δ = 2.76 (s, 2H), 2.69 (s, 1H), 2.45 (s, 1H), 2.25 (d, J = 12.5 Hz, 2H), 2.21 (s, 4H), 2.16 (s, 4H) ppm; ^{13}C NMR (125 MHz, CS_2 (C_6D_6 in capillary), 293 K): not obtained because of the low solubility; MALDI-TOF MS (matrix = 1,1,4,4-tetraphenyl-1,3-butadiene) *m/z* 1243 ([*M*]$^-$).

Crystal Data for 4b/4c. $Sc_3NC_{90}H_{14}\cdot 0.72(C_6H_4Cl_2)\cdot 1.06(CS_2)$, M_w = 1430.37, crystal size: 0.161 × 0.139 × 0.117 mm, monoclinic, $P2_1/n$, a = 11.1426(3) Å, b = 21.8822(6) Å, c = 20.6043(5) Å, β = 98.677(1)°, V = 4966.3(2) Å^3, Z = 4, D_{calc} = 1.913 g/cm^3, μ = 0.637 mm^{-1}, T = 90 K, 47360 reflections, 18838 unique reflections; 14984 with $I > 2\sigma(I)$; R_1 = 0.0692 [$I > 2\sigma(I)$], wR_2 = 0.1891 (all data), GOF (on F^2) = 1.074. The maximum residual electron density is equal to 1.718 e Å^{-3}.

Synthesis of Ad Bis-adducts of $Lu_3N@I_h$-C_{80}. A 26 mL aliquot of a 1,2-DCB solution of **3a** (2.6 mg, 6.0 × 10^{-5} M) and 200 equiv. of **1** (52 mg, 1.2 × 10^{-2} M) were placed in a Pyrex tube. After degassing using three freeze–pump–thaw cycles under reduced pressures, the mixture was irradiated with a high-pressure mercury lamp through a cutoff filter (cutoff < 350 nm) under argon atmosphere for 5 min. The conversion yields of the bis-adducts were estimated as 70% using the HPLC peak area. The residue was then purified by HPLC using a Buckyprep column (20 mm × 250 mm i.d., Nacalai Tesque Inc.; eluent, toluene) followed by a recycling procedure using a 5NPE column (20 mm × 250 mm i.d., Nacalai Tesque Inc.; eluent, toluene) and afforded isolation of two Ad bis-adduct isomers **5a** and **5b**, although the amounts of the isolated samples were extremely small.

Spectral Data for 5a. ^{1}H NMR (500 MHz, CS_2 (C_6D_6 in capillary), 293 K) δ = 3.25–3.16 (m, 4H), 3.02–2.85 (m. 8H), 2.57–2.39 (m, 16H) ppm; ^{13}C NMR (125 MHz, CS_2 (C_6D_6 in capillary), 293 K): not obtained because of the low solubility; MALDI-TOF MS (matrix = 1,1,4,4-tetraphenyl-1,3-butadiene) *m/z* 1767 ([*M*]$^-$).

Spectral Data for 5b. ^{1}H NMR (500 MHz, CS_2 (C_6D_6 in capillary), 293 K) δ = 3.13–2.87 (m, 12H), 2.58–2.39 (m. 16H), 2.57–2.39 (m, 16H) ppm; ^{13}C NMR (125 MHz, CS_2 (C_6D_6 in capillary), 293 K): not obtained because of the low solubility; MALDI-TOF MS (matrix = 1,1,4,4-tetraphenyl-1,3-butadiene) *m/z*

1767 ([*M*]–).

Crystal Data for 5b. $Lu_3NC_{100}H_{28}$, M_w = 1768.14, crystal size: 0.250 × 0.090 × 0.050 mm, monoclinic, *P*2/*n*, *a* = 11.8051(13) Å, *b* = 11.2255(12) Å, *c* = 18.615(2) Å, β = □9□□□□5□3□°, *V* = 2466.8(5) Å^3, *Z* = 2, D_{calc} = 2.380 g/cm^3, μ = 6.031 mm^{-1}, *T* = 90 K, 9149 reflections, 8462 unique reflections; 7363 with $I > 2\sigma(I)$; R_1 = 0.0458 [$I > 2\sigma(I)$], wR_2 = 0.1365 (all data), GOF (on F^2) = 1.113. The maximum residual electron density is equal to 4.41 eÅ^{-3}.

CCDC 1522864 (**2a**), CCDC 1522865 (**2b**), CCDC 1522866 (**3a**), CCDC 1522867 (**3b**), CCDC 1522868 (**4a**), CCDC 1522869 (**4b/4c**), and CCDC 1522870 (**5b**) contain the supplementary crystallographic data for this paper. These data can be obtained free of charge by The Cambridge Crystallographic Data Centre.

Computational details. All calculations were conducted using the Gaussian 09 program.[33] Geometry optimization and vibrational frequency analyses were performed with density functional theory (DFT) at the B3LYP[34] level using the 6-31G(d) basis set[35] on H, N, and C atoms and the SDD basis set[36] (with the SDD effective core potential) for Sc and Lu. Mulliken atomic charges and POAV[29] values were calculated also in the B3LYP/6-31G(d)~SDD optimized structures (charges using the recommended B3LYP/3-21G~SDD approach[29c]).

Acknowledgements

This work was supported by a Grant-in-Aid for Scientific Research on Innovative Areas (No. 20108001, "pi-Space"), a Grant-in-Aid for Scientific Research (A) (No. 202455006) and (B) (No. 24350019), Specially Promoted Research (No. 22000009) from the Ministry of Education, Culture, Sports, Science, and Technology of Japan. S.S. thanks the Japan Society for the Promotion of Science (JSPS) for the Research Fellowship for Young Scientists. A.L.B. and M.M.O. thank the US National Science Foundation (Grant CHE-1305125) for financial support.

Keywords: Fullerenes • X-ray diffraction • Cycloaddition • Regioselectivity • Rare Earths

[1] S. Stevenson, G. Rice, K. Harich, F. Cromer, M. R. Jordan, J. Craft, E. Hadju, R. Bible, M. M. Olmstead, K. Maitra, A. J. Fisher, A. L. Balch, H.

C. Dorn, *Nature* **1999**, *401*, 55-57.

[2] a) S. Stevenson, M. C. Thompson, H. L. Coumbe, M. A. Mackey, C. E. Coumbe and J. P. Phillips, *J. Am. Chem. Soc.* **2007**, *129*, 16257-16262; b) S. Stevenson, M. A. Mackey, M. C. Thompson, H. L. Coumbe, P. K. Madasu, C. E. Coumbe, J. P. Phillips, *Chem. Commun.* **2007**, 4263-4265.

[3] a) Z. X. Ge, J. C. Duchamp, T. Cai, H. W. Gibson, H. C. Dorn, *J. Am. Chem. Soc.* **2005**, *127*, 16292-16298; b) S. Stevenson, K. Harich, H. Yu, R. R. Stephen, D. Heaps, C. Coumbe, J. P. Phillips, *J. Am. Chem. Soc.* **2006**, *128*, 8829-8835; c) S. Stevenson, M. A. Mackey, C. E. Coumbe, J. P. Phillips, B. Elliott, L. Echegoyen, *J. Am. Chem. Soc.* **2007**, *129*, 6072-6073; d) C. D. Angeli, T. Cai, J. C. Duchamp, J. E. Reid, E. S. Singer, H. W. Gibson, H. C. Dorn, *Chem. Mater.* **2008**, *20*, 4993-4997.

[4] a) D. Rivera-Nazario, J. R. Pinzón, S. Stevenson, L. A. Echegoyen, *J. Phys. Org. Chem.* **2013**, *26*, 194-205; b) J. Zhang, S. Stevenson, H. C. Dorn, *Acc. Chem. Res.* **2013**, *46*, 1548-1557.

[5] a) R. B. Ross, C. M. Cardona, D. M. Guldi, S. G. Sankaranarayanan, M. O. Reese, N. Kopidakis, J. Peet, B. Walker, G. C. Bazan, E. Van Keuren, B. C. Holloway, M. Drees, *Nat. Mater.* **2009**, *8*, 208-212. b) L. Feng, M. Rudolf, S. Wolfrum, A. Troeger, Z. Slanina, T. Akasaka, S. Nagase, N. Martín, T. Ameri, C. J. Brabec, D. M. Guldi, *J. Am. Chem. Soc.* **2012**, *134*, 12190–12191.

[6] a) P. P. Fatouros, F. D. Corwin, Z.-J. Chen, W. C. Broaddus, J. L. Tatum, B. Kettenmann, Z. Ge, H. W. Gibson, J. L. Russ, A. P. Leonard, J. C. Duchamp, H. C. Dorn, *Radiology* **2006**, *240*, 756-764; b) J. Zhang, P. P. Fatouros, C. Shu, J. Reid, L. S. Owens, T. Cai, H. W. Gibson, G. L. Long, F. D. Corwin, Z.-J. Chen, H. C. Dorn, *Bioconjugate Chem.* **2010**, *21*, 610-615; c) H. L. Fillmore, M. D. Shultz, S. C. Henderson, P. Cooper, W. C. Broaddus, Z. J. Chen, C. Y. Shu, J. F. Zhang, J. C. Ge, H. C. Dorn, F. Corwin, J. I. Hirsch, J. Wilson, P. P. Fatouros, *Nanomedicine* **2011**, *6*, 449-458.

[7] M. D. Shultz, J. C. Duchamp, J. D. Wilson, C.-Y. Shu, J. Ge, J. Zhang, H. W. Gibson, H. L. Fillmore, J. I. Hirsch, H. C. Dorn, P. P. Fatouros, *J. Am. Chem. Soc.* **2010**, *132*, 4980-4981.

[8] a) E. B. Iezzi, J. C. Duchamp, K. Harich, T. E. Glass, H. M. Lee, M. M. Olmstead, A. L. Balch, H. C. Dorn, *J. Am. Chem. Soc.* **2002**, *124*, 524-525;

b) H. M. Lee, M. M. Olmstead, E. Iezzi, J. C. Duchamp, H. C. Dorn, A. L. Balch, *J. Am. Chem. Soc.* **2002**, *124*, 3494-3495.

[9] a) C. M. Cardona, A. Kitaygorodskiy, L. Echegoyen, *J. Am. Chem. Soc.* **2005**, *127*, 10448-10453; b) O. Lukoyanova, C. M. Cardona, J. Rivera, L. Z. Lugo-Morales, C. J. Chancellor, M. M. Olmstead, A. Rodríguez-Fortea, J. M. Poblet, A. L. Balch, L. Echegoyen, *J. Am. Chem. Soc.* **2007**, *129*, 10423-10430; c) J. R. Pinzón, T. Zuo, L. Echegoyen, *Chem. –Eur. J.* **2010**, *16*, 4864-4869.

[10] a) C. M. Cardona, A. Kitaygorodskiy, A. Ortiz, Á. Herranz, L. Echegoyen, *J. Org. Chem.* 2005, **70**, 5092; b) T. Cai, Z. Ge, E. B. Iezzi, T. E. Glass, K. Harich, H. W. Gibson, H. C. Dorn, *Chem. Commun.* **2005**, 3594-3596; c) A. Rodríguez-Fortea, J. M. Campanera, C. M. Cardona, L. Echegoyen, J. M. Poblet, *Angew. Chem. Int. Ed.* **2006**, *45*, 8176-8180; d) L. Echegoyen, C. J. Chancellor, C. M. Cardona, B. Elliott, J. Rivera, M. M. Olmstead, A. L. Balch, *Chem. Commun.* **2006**, 2653-2655; e) C. M. Cardona, B. Elliott, L. Echegoyen, *J. Am. Chem. Soc.* **2006**, *128*, 6480-6485; f) T. Cai, C. Slebodnick, L. Xu, K. Harich, T. E. Glass, C. Chancellor, J. C. Fettinger, M. M. Olmstead, A. L. Balch, H. W. Gibson, H. C. Dorn, *J. Am. Chem. Soc.* **2006**, *128*, 6486-6492; g) S. Aroua, Y. Yamakoshi, *J. Am. Chem. Soc.* **2012**, *134*, 20242-20245; h) S. Aroua, M. Garcia-Borras, S. Osuna, Y. Yamakoshi, *Chem. –Eur. J.* **2014**, *20*, 14032-14039; i) Y. Maeda, M. Kimura, C. Ueda, M. Yamada, T. Kikuchi, M. Suzuki, W.-W. Wang, N. Mizorogi, N. Karousis, N. Tagmatarchis, T. Hasegawa, M. M. Olmstead, A. L. Balch, S. Nagase, T. Akasaka, *Chem. Commun.* **2014**, 50, 12552-12555.

[11] a) F.-F. Li, J. R. Pinzón, B. Q. Mercado, M. M. Olmstead, A. L. Balch, L. Echegoyen, *J. Am. Chem. Soc.* **2011**, *133*, 1563-1571; b) G.-W. Wang, T.-X. Liu, M. Jiao, N. Wang, S.-E. Zhu, C. Chen, S. Yang, F. L. Bowles, C. M. Beavers, M. M. Olmstead, B. Mercado, A. L. Balch, *Angew. Chem.* **2011**, *123*, 4754-4758; *Angew. Chem. Int. Ed.* **2011**, *50*, 4658-4662.

[12] a) C. Shu, W. Xu, C. Slebodnick, H. Champion, W. Fu, J. E. Reid, H. Azurmendi, C. Wang, K. Harich, H. C. Dorn, H. W. Gibson, *Org. Lett.* **2009**, *11*, 17531756; b) M. Izquierdo, M. R. Cerón, M. M. Olmstead, A. L. Balch, L. Echegoyen, *Angew. Chem.* **2013**, *125,* 12042-12046; *Angew. Chem. Int. Ed.*

2013, 52, 11826-11830.

[13] a) C. Shu, T. Cai, L. Xu, T. Zuo, J. Reid, K. Harich, H. C. Dorn, H. W. Gibson, *J. Am. Chem. Soc.* **2007**, *129*, 15710-15717; b) C. Shu, C. Slebodnick, L. Xu, H. Champion, T. Fuhrer, T. Cai, J. E. Reid, W. Fu, K. Harich, H. C. Dorn, H. W. Gibson, *J. Am. Chem. Soc*. **2008**, *130*, 17755-17560.

[14] a) T. Wakahara, Y. Iiduka, O. Ikenaga, T. Nakahodo, A. Sakuraba, T. Tsuchiya, Y. Maeda, M. Kako, T. Akasaka, K. Yoza, E. Horn, N. Mizorogi, S. Nagase, *J. Am. Chem. Soc.* **2006**, *128*, 9919-9925; b) M. Kako, K. Miyabe, K. Sato, M. Suzuki, N. Mizorogi, W.-W. Wang, M. Yamada, Y. Maeda, M. M. Olmstead, A. L. Balch, S. Nagase, T. Akasaka, *Chem. –Eur. J.* **2015**, *21*, 16411-16420.

[15] K. Sato, M. Kako, M. Suzuki, N. Mizorogi, T. Tsuchiya, M. M. Olmstead, A. L. Balch, T. Akasaka, S. Nagase, *J. Am. Chem. Soc*. **2012**, *134*, 16033-16039.

[16] T.-X. Liu, T. Wei, S.-E. Zhu, G.-W. Wang, M. Jiao, S. Yang, F. L. Bowles, M. M. Olmstead, A. L. Balch, *J. Am. Chem. Soc.* **2012**, *134*, 11956-11959.

[17] M. Yamada, T. Akasaka, S. Nagase, *Chem. Rev.* **2013**, *113*, 7209-7264.

[18] M. Yamada, T. Akasaka, *Bull. Chem. Soc. Jpn.* **2014**, *87*, 1289-1314.

[19] For a prominent example, see: Y. Iiduka, T. Wakahara, T. Nakahodo, T. Tsuchiya, A. Sakuraba, Y. Maeda, T. Akasaka, K. Yoza, E. Horn, T. Kato, M. T. H. Liu, N. Mizorogi, K. Kobayashi, S. Nagase, *J. Am. Chem. Soc.* **2005**, *127*, 12500-12501.

[20] S. Sato, Seki, Y. Honsho, L. Wang, H. Nikawa, G. Luo, J. Lu, M. Haranaka, T. Tsuchiya, S. Nagase, T. Akasaka, *J. Am. Chem. Soc.* **2011**, *133*, 2766-2771.

[21] J. C. Duchamp, A. Demortier, K. R. Fletcher, D. Dorn, E. B. Iezzi, T. Glass, H. C. Dorn, *Chem. Phys. Lett.* **2003**, *375*, 655-659.

[22] a) T. Cai, L. Xu, M. R. Anderson, Z. Ge, T. Zuo, X. Wang, M. M. Olmstead, A. L. Balch, H. W. Gibson, H. C. Dorn, *J. Am. Chem. Soc*. **2006**, *128*, 8581-8589; b) M. R. Ceron, M. Izquierdo, N. Alegret, J. A. Valdez, A. Rodríguez-Fortea, M. M. Olmstead, A. L. Balch, J. M. Poblet, L. Echegoyen, *Chem. Commun.* **2016**, *52*, 64-67.

[23] S. Osuna, R. Valencia, A. Rodríguez-Fortea, M. Swart, M. Solà, J. M. Poblet, *Chem. – Eur. J.* **2012**, *18*, 8944-8956.

[24] a) S. Stevenson, R. R. Stephen, T. M. Amos, V. R. Cadorette, J. E. Reid, J. P. Phillips, *J. Am. Chem. Soc.* **2005**, *127*, 12776-12777; b) T. Cai, L. Xu, C. Shu, H. A. Champion, J. E. Reid, C. Anklin, M. R. Anderson, H. W. Gibson, H. C. Dorn, *J. Am. Chem. Soc.* **2008**, *130*, 2136-2137; c) S. Aroua, M. Garcia-Borràs, M. F. Bölter, S. Osuna, Y. Yamakoshi, *J. Am. Chem. Soc.* **2015**, *137*, 58-61; d) M. Cerón, M. Izquierdo, M. Garcia-Borràs, S. S. Lee, S. Stevenson, S. Osuna, L. Echegoyen, *J. Am. Chem. Soc.* **2015**, *137*, 11775-11782.

[25] M. Yamada, C. Someya, T. Wakahara, T. Tsuchiya, Y. Maeda, T. Akasaka, K. Yoza, E. Horn, M. T. H. Liu, N. Mizorogi, S. Nagase, *J. Am. Chem. Soc.* **2008**, *130*, 1171-1176.

[26] P. Bao, B. Liu, X. Li, C. Pan, Y. Xie, X. Lu, *Dalton Trans.* **2016**, *45*, 11606-11610.

[27] S. Osuna, A. Rodríguez-Fortea, J. M. Poblet, M. Solà, M. Swart, *Chem. Commun*. **2012**, *48*, 2486-2488.

[28] S. Yang, A. A. Popov, L. Dunsch, *Angew. Chem.* **2008**, *120*, 8318-8322; *Angew. Chem. Int. Ed*. **2008**, *47*, 8196-8200.

[29] a) R. C. Haddon, *Science* **1993**, *261*, 1545-1550; b) R. C. Haddon, *J. Am. Chem. Soc.* **1998**, *119*, 1797-1798; c) Z. Slanina, F. Uhlík, S.-L. Lee, L. Adamowicz, T. Akasaka, S. Nagase, *J. Comput. Theor. Nanosci.* **2011**, *8*, 2233-2239.

[30] X. Lu, H. Nikawa, T. Tsuchiya, Y. Maeda, M. O. Ishitsuka, T. Akasaka, M. Toki, H. Sawa, Z. Slanina, N. Mizorogi, S. Nagase, *Angew. Chem.* **2008**, *120*, 8770-8773; *Angew. Chem. Int. Ed.* **2008**, *47*, 8642-8645.

[31] M. O. Ishitsuka, S. Sano, H. Enoki, S. Sato, H. Nikawa, T. Tsuchiya, Z. Slanina, N. Mizorogi, M. T. H. Liu, T. Akasaka, S. Nagase, *J. Am. Chem. Soc.* **2011**, *133*, 7128-7134.

[32] F. Cozzi, W. H. Powell, C. Thilgen, *Pure Appl. Chem.* **2005**, 77, 843-923.

[33] Gaussian 09, Revision A.02 & D.01, M. J. Frisch, G. W. Trucks, H. B.

Schlegel, G. E. Scuseria, M. A. Robb, J. R. Cheeseman, G. Scalmani, V. Barone, B. Mennucci, G. A. Petersson, H. Nakatsuji, M. Caricato, X. Li, H. P. Hratchian, A. F. Izmaylov, J. Bloino, G. Zheng, J. L. Sonnenberg, M. Hada, M. Ehara, K. Toyota, R. Fukuda, J. Hasegawa, M. Ishida, T. Nakajima, Y. Honda, O. Kitao, H. Nakai, T. Vreven, J. A. Montgomery Jr., J. E. Peralta, F. Ogliaro, M. Bearpark, J. J. Heyd, E. Brothers, K. N. Kudin, V. N. Staroverov, R. Kobayashi, J. Normand, K. Raghavachari, A. J. Rendell, C. Burant, S. S. Iyengar, J. Tomasi, M. Cossi, N. Rega, J. M. Millam, M. Klene, J. E. Knox, J. B. Cross, V. Bakken, C. Adamo, J. Jaramillo, R. Gomperts, R. E. Stratmann, O. Yazyev, A. J. Austin, R. Cammi, C. Pomelli, J. W. Ochterski, R. L. Martin, K. Morokuma, V. G. Zakrzewski, G. A. Voth, P. Salvador, J. J. Dannenberg, S. Dapprich, A. D. Daniels, O. Farkas, J. B. Foresman, J. V. Ortiz, J. Cioslowski, D. J. Fox, Gaussian, Inc., Wallingford, CT, **2009**.

[34] a) A. D. Becke, *Phys. Rev. A* **1988**, *38*, 3098-3100; b) A. D. Becke, *J. Chem. Phys.* **1993**, *98*, 5648-5652; c) C. Lee, W. Yang, R. G. Parr, *Phys. Rev. B* **1988**, *37*, 785-789.

[35] W. J. Hehre, R. Ditchfield, J. A. Pople, *J. Chem. Phys.* **1972**, *56*, 2257-2261.

[36] X. Y. Cao, M. Dolg, *THEOCHEM* **2002**, *581*, 139-147.